PUBLISHED BY IOP PUBLISHING FOR SISSA

RECEIVED: *October 31, 2011*
ACCEPTED: *January 6, 2012*
PUBLISHED: *February 9, 2012*

THE 9th INTERNATIONAL CONFERENCE ON POSITION SENSITIVE DETECTORS,
12–16 SEPTEMBER 2011,
ABERYSTWYTH, U.K.

EIGER a new single photon counting detector for X-ray applications: performance of the chip

V. Radicci,[a,b,1] A. Bergamaschi,[a] R. Dinapoli,[a] D. Greiffenberg,[a] B. Henrich,[a] I. Johnson,[a] A. Mozzanica,[a] B. Schmitt[a] and X. Shi[a]

[a] *Paul Scherrer Institut,*
5232 Villigen PSI, Switzerland
[b] *European Synchrotron Radiation Facility,*
6 Rue J. Horowitz, 38043 Grenoble, France

E-mail: valeria.radicci@psi.ch

ABSTRACT: EIGER is the next generation of single photon counting pixel detector for synchrotron radiation designed by the PSI-SLS detector group. It features a pixel size of 75×75 μm^2 and frame rates up to 23 kHz. The chip contains 256×256 pixels, has a total size of 19.3×20 mm^2 and provides 4, 8 and 12 bit counting modes. This dynamic range is extendable to 32 bits with continuous read/write and summation of frames on the fly in firmware.

Along with X-ray absorption images, the characterization and performance of the chip is presented. The energy calibration, noise, minimum energy threshold and rate capability measured with a single chip test system in a X-ray tube and at the SLS-PSI synchrotron are shown. Trimming studies and irradiation effects are discussed as well. To conclude, the status of the production of larger detector systems consisting of 2×4 chip modules and multi modules detector systems (9 Mpixels; 3×6 modules) is outlined.

KEYWORDS: X-ray detectors; Si microstrip and pad detectors; Instrumentation for synchrotron radiation accelerators

[1] Corresponding author.

doi:10.1088/1748-0221/7/02/C02019

Contents

2012 JINST 7 C02019

1 Introduction

EIGER [1] is a single photon counting detectors [2, 3] being developed by the PSI-SLS detector group for diffraction experiments at synchrotron light sources like protein crystallography, coherent small angle X-ray scattering, coherent diffraction imaging, X-ray photon correlation spectroscopy [4–6].

The EIGER detector design, with a small pixel size 75×75 μm^2 and the possibility of reading out during an exposure, fulfils the main requirements for those experiments: good spatial resolution and fast frame rate. Moreover, an ideal detector for those kind of applications should also detect all incident photons without intrinsic noise, should have high dynamic range, no spatial distortion and uniform response at wavelengths ranging from a few keV to 20 keV [2].

2 Description of the EIGER detector

EIGER is a hybrid detector consisting of p+ pixelized implants on a 300 μm n-silicon substrate, bump-bonded to a Read Out Chip (ROC). The ROC has 256×256 pixels of 75×75 μm^2 and a total size of 19.3×20 mm^2. A detailed description of the main features of the ROC, the pixel architecture and the chip readout scheme is reported in [1].

The charge produced in the silicon substrate by the incoming photon is collected at the pixel implants and read out through the ROC. In the read out chain the charge is first amplified with a low noise amplifier and then shaped through a shaper. Both components have a tunable shaping time and gain to allow different modes of operation depending on the experimental requirements:

1. *Low noise mode* with high gain, used mainly in the low energy range;

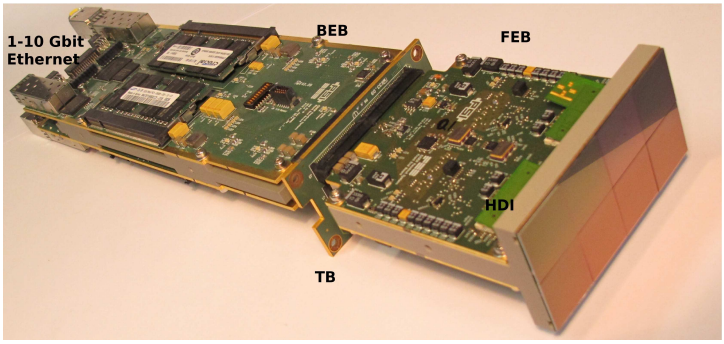

Figure 1. Picture of a full EIGER module.

2. *Standard mode* with an intermediate gain;

3. *Fast mode* with a shaped signal small in amplitude but fast in return to zero time, suitable for high rate experiments.

The so shaped signal is then compared with a threshold and if higher, the pixel digital counter is incremented by one. The comparator threshold is given by a global reference voltage (V_{cmp}) plus a voltage individually adjustable on each pixel with 6-bit DACs in order to compensate the pixel to pixel variations. The binary counter is configurable in 4 bits, 8 bits and 12 bits. In applications with longer exposure time the dynamic range can be extended to 32 bits with continuous read/write and summation of several images on the readout control board.

At the end of the exposure the counters are read out through the chip in the following way: a token travels in a side shift register selecting all the pixels in a row, which in parallel send the information to the column periphery readout logic. Actually, it is possible to select the row three times according to the configuration of the counter bit. When selected the first time, the information of the 256×4 bit counters in the row are transferred to the periphery and if the chip is operated in 8 or 12 bit mode, the second and eventually the third group of 4 bit counters are then transferred, otherwise the token passes directly to the next row. With this scheme the 4 bit mode is the fastest mode to read the ROC. It takes in fact only $t_{\mathrm{ROmin}} = 41\ \mu$s. At the column periphery the information of eight successive columns is serialized onto a single output pad. In total 32 serializers are implemented in the ROC. Every serializer sends the data to an I/O driver with a 100 MHz Double Data Rate (DDR) clock.

One of the main EIGER novel features is the possibility of reading out the chip while acquiring a subsequent exposure. This is possible due to an on-pixel storing buffer, where the information of each counter is temporarily stored. The main counter can then be reset and a new exposure can be started while the buffer information is read out. In summary, storing the bit information, resetting the counter and enabling the pixel for the second exposure takes about $t_{\mathrm{dead}} \simeq 3\mu$s. That is basically the dead time of the chip. Operating the chip in 4 bit and parallel readout mode EIGER can achieve the fastest frame rate of around $1/(t_{\mathrm{ROmin}} + t_{\mathrm{dead}}) \simeq 23$ kHz.

The basic element of an EIGER detector is the module. It consists of a matrix of 2×4 read out chips bump-bonded to a monolithic silicon sensor of 77×39 mm^2. The module is read out through two separate, back to back, read out chains each one serving 4 chips (a half module) (figure 1).

2012 JINST 7 C02019

Eight chips bump-bonded to the silicon sensor are glued and wirebonded to a flexible printed circuit board the *High Density Interconnect Board* (HDI), which addresses the signals from the ROCs to the Frontend Board (FEB). Two FPGAs on the FEB generate the control signals for the ROCs and reorganize the output data to be sent to the Backend Board (BEB). A transition board (TB) connects the FEB to the BEB and delivers the power to the whole system. Finally the BEB transmits the data to the control PC. A standard 1 and 10 Gb ethernet connection is used respectively for the slow control of the module and for the data flow. The read out chain at the top of the module, visible in figure 1, consists of a FEB, TB, BEB and serves the four top chips; the one at the bottom serves the other four chips and runs in parallel to the first one. Each module has in total four ethernet connections.

An EIGER detector consists of several single modules tiled together. Thanks to the high parallelism in the data acquisition system the frame rate capability of the detector will be the same of the chip. Depending on the experiment requirements and the sensitive area to be covered, detectors from a single module (77×39 mm^2 and $\simeq 0.5$ Mpixels) to many module systems (like a 0.25×0.25 cm^2 and 9 Mpixels) are planned.

3 Single chip calibration and testing

A detailed analysis of the EIGER chip is ongoing to optimize and calibrate the DAC parameters for the three different modes of operation (*Low noise*, *Standard* and *Fast mode*) and to measure the main detector characteristics such as energy calibration, noise, threshold dispersion, rate capability and minimum energy. Moreover, in order to guarantee the uniformity of the chip response, an effective trimming procedure for the pixel threshold equalization is being studied and validated.

For these purposes a dedicated single chip test setup was developed. It consists of an adapter board, where a single chip is glued and wire-bonded, connected to a Chip Test Board (CTB) which generates the supply voltages and the control signals for the chip, reads back the data and transfers them to the computer through a standard ethernet data link.

Several bump-bonded chips have been tested with an X-ray tube and fluorescent targets over an energy range from 2.6 keV (Cl) to 22.2 keV (Ag); one has also been tested at the PSI SLS-Optics beam line [7] in a energy range from 10 keV to 16 keV. The monochromatic, intense, uniform and localized beam at the beam line has allowed us to perform an irradiation of a pixel region (1300 pixels $\simeq 7$ mm^2) up to a dose of $\simeq 6$ MRad and of a row and column periphery region up to $\simeq 16$ MRad.

3.1 Energy calibration

In single photon counting detectors the number of counts in each pixel corresponds to the number of incoming photons which have generated a signal greater than the comparator threshold. The signal produced by a photon is proportional to the charge Q deposited in the silicon, which depends on the photon energy E_ϕ. Thus the calibration of the comparator threshold in terms of energy (eV) is extremely important. Moreover the comparator level to choose for a particular photon energy (E_ϕ) is crucial to obtain good quality data. The total charge Q, in fact, can be either collected by a single pixel with a signal proportional to Q or shared between two or more pixels; in case of sharing between two pixels, the one closer to the photon impact point measures a signal $Q/2 \leq Q^{'} \leq Q$, the further a signal $0 \leq Q^{'} \leq Q/2$ accordingly to its proximity. For monochromatic beam, in order

2012 JINST 7 C02019

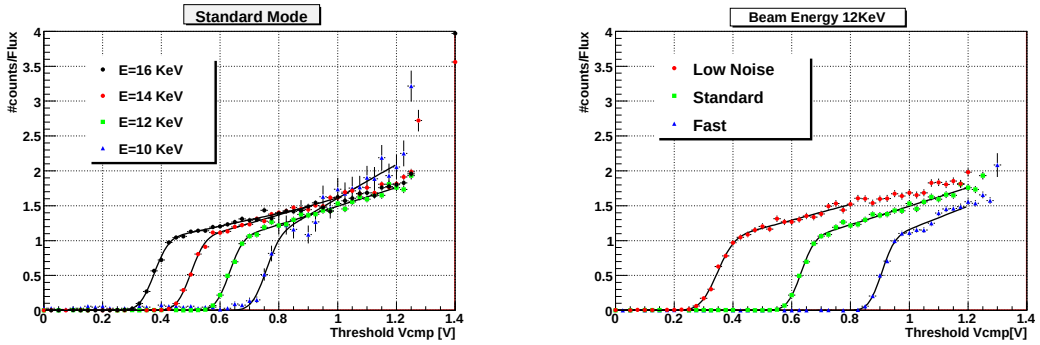

(a) (b)

Figure 2. Single pixel threshold scans at the Optics beam line: (a) for different X-ray energies and the chip operated in *Standard mode* (b) at 12 keV and the chip operated in the three different gain modes. Low values of the threshold in Volt correspond to higher threshold in energy.

to efficiently count all the incoming photons (both the ones absorbed in single pixel and the shared ones) but to avoid double counting, the comparator threshold should be precisely set to a charge level $Q/2 \propto E_\phi/2$.

The standard procedure for the energy calibration described in detail in [3] and [8] starts with a so-called *threshold scan* where the number of counts in monochromatic beam is recorded as a function of the comparator threshold ($V_{\rm cmp}$). Ideally the threshold scan should follow a step function: if the signal is higher or equal to the threshold then photons are detected. The transition threshold is called *inflection point* and is proportional to E_ϕ. Actually, due to the electronic noise and the energy distribution of the incoming photons, the step is smeared around this point giving an *S-curve*. Moreover for an energy threshold lower than the inflection point the number of counts constantly increases due to the shared photons with a lower signal on the pixels. The following equation describes the observed behavior and basically consists of an S-curve multiplied by a linear *charge sharing term*:

$$n(V_{\rm cmp}) = \frac{1}{2}\left(1+\mathrm{erf}\left(\frac{V_{\rm cmp}-a_1}{\sqrt{2}a_2}\right)\right)((a_3+a_4(V_{\rm cmp}-a_1)) \tag{3.1}$$

where a_1 is the inflection point; a_2 is the *noise* related to the electronic noise of the chip, the X-ray energy spectrum and the charge sharing effect; a_3 is the number of counts at the inflection point depending on the flux and the exposure time and a_4 is the slope of the charge sharing contribution.

As an example, figure 2 shows some threshold scans on a single pixel. In particular, the curves in figure 2-(a) shows the behavior of a pixel, in *Standard mode*, illuminated with photons of different energies from 10 keV to 16 keV. In figure 2-(b) photons of 12 keV are used to scan the threshold for three different gains of the charge sensitive preamplifier. All curves are fitted with eq. (3.1). It is important to notice that low values of the comparator voltage $V_{\rm cmp}$ expressed in Volt correspond to high threshold in energy. Therefore when the threshold is low enough ($V_{\rm cmp} \simeq 1.2$V) to be compared to the noise level, the number of counts suddenly increases due to the pixel crosstalk. This point is called *minimum threshold*. As expected, the higher the energy the lower (in Volt) is the inflection point (figure 2-(a)).

2012 JINST 7 C02019

Table 1. Summary of EIGER measurements in the three different mode of the operation: gain slope, gain offset, minimum energy threshold, noise and dead time.

Operation Mode	**Gain Slope** (mV/keV)	**Gain Offset** (mV)	**Minimum Engergy Threshold** (keV)	**Noise** (e^-)	**Dead Time** (ns)
Fast	-49.60 ± 0.02	1514.2 ± 0.3	7.5	185 ± 19	238.2 ± 0.2
Standard	-69.02 ± 0.04	1454.0 ± 0.4	4.9	160 ± 14	251.6 ± 0.3
Low noise	-91.7 ± 0.1	1412 ± 1	$\simeq 4$	121 ± 11	304.2 ± 0.8

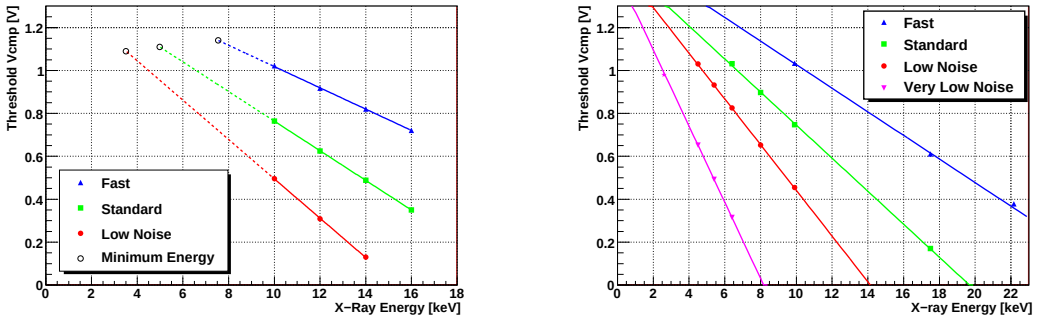

(a) (b)

Figure 3. (a) Energy calibration measured at Optics beam line on a single chip in three mode of operation; (b) Energy calibration measured with an X-ray Cu tube and fluorescent targets the chip is operated with three different gains of the preamplifier plus a *Very low noise mode*.

To complete the energy calibration, the inflection point measured on each pixel is plotted as a function of E_ϕ and fitted with a linear function to extract the *gain slope* and *gain offset*. Finally the mean and the sigma of both the gain slope and gain offset distribution are evaluated.

A calibration has been performed with a single EIGER chip at the Optics beam line with a monochromatic beam with an energy ranging from 10 keV to 16 keV. Figure 3-(a) shows the calibration curves in three mode of operation of the chip: *Low noise*, *Standard* and *Fast*; the range of the linear fit is from 10 to 16 keV. Supposing the comparator linear down to low energies, the calibration lines are extrapolated up to the minimum threshold $\simeq 1.1$ V. The open dots in figure 3-(a) are the *minimum energy threshold* that could be set for EIGER. Table 1 lists the values of the gain slope, the gain offset and the minimum energy threshold for the three mode of operation of the chip.

3.2 Low energy operation

The linearity of the comparator and its behavior at low energies have been studied with X-rays from a Cu tube and different target materials to produce fluorescence peaks in a range of energies from 2.6 keV (chlorine target) to 22.2 keV (silver target). In figure 3-(b) the calibration curves are plotted. Also a further higher gain of the preamplifier, called *Very low noise*, has been used to be sensitive to the lowest energy photons (2.6 keV). The plot clearly shows the very good performance of the chip at low energies and, in particular, the comparator shows a high linearity in the whole range

2012 JINST 7 C02019

of V_{cmp} from 0.2 V to $\simeq$1.1 V for all the different preamplifier settings. With an energy threshold as low as 2.5 keV in the highest gain mode it is possible to count fluorescent photons from chlorine.

3.3 Trimming procedure

Due to the differences in the comparator thresholds in the pixels on the same chip, the inflection point distribution has a dispersion $\simeq$480 eV. Differences in the threshold imply non uniformity in the pixel response to a monochromatic beam and result in a degradation of the image quality. Therefore, the comparator threshold is tunable for each individual pixel. The threshold of the comparator consists in fact of two parts: a global voltage V_{cmp} to be set at chip level and an individual offset that is controlled with a 6 trim bit DAC adjustable at the pixel level, times a global V_{trim} voltage, which sets the strengths of the trim bits. Several trimming procedures can be applied. Typically threshold scans with monochromatic beam are repeated for all the possible 64 trim values and are fitted with S-curves. The trim bit value which gives the inflection point closer to the mean of the untrimmed distribution is then chosen. This procedure is very time consuming in particular with EIGER with 65536 channels and 64 trim values.

Therefore, a new and faster procedure has been developed and tested. First of all, a single threshold scan is done with all the trim bits set at the middle of the range (32) and V_{trim} =1.35 V, lowest effective value for the trim bit strength. After the scan, the S-curves are fitted and the mean (A_1) of the inflection point distribution and the mean (N_1) of the number of counts at the inflection point are evaluated. Then the pixel trim bits are moved around until the number of counts on each pixel at $V_{cmp} = A_1$ is equalized to N_1. With this procedure, it is very important that the beam is not only monochromatic but also uniform on the whole chip, both conditions are easily obtained with X-rays from fluorescence. In figure 4-(a) and (b) the S-curves measured on four different pixels before and after trimming are plotted. After trimming the four experimental curves merge completely indicating the correctness of the procedure developed. The effectiveness of this trimming procedure is evident also from the comparison of the threshold distributions before and after trimming (figure 5). Thereby, the sigma of the threshold distributions called *Threshold dispersion* measured in standard settings with X-rays from Cu fluorescence (8 keV) improves from 479 eV, before trimming, to 67 eV after trimming.

With the chosen V_{trim} less then 1% of the pixel cannot be trimmed, by slightly increasing the V_{trim} strenght all the pixels could be trimmed worsening by $\simeq$ 10% the threshold dispersion. Studies for the V_{trim} optimization as a function of beam energy and gain are in progress.

3.4 Noise

The electronic noise of the chip can be estimated through the parameter a_2 of eq. (3.1). Actually, this parameter depends both on the chip noise and on the energy dispersion of the X-ray beam. The energy dispersion contribution can be neglected using a monochromatic beam. The noise has been measured at the Optics beam line with an energy of 14 keV free from higher energy contributions [7].

The procedure for the noise estimation starts with a threshold scan fitted with eq. (3.1). The parameter a_2, expressed in Volt, is then turned into energy using the energy calibration, then the noise in eV is converted in e^- taking into account that each photon creates in average $E_\phi/3.63$ eV electron-hole pairs.

2012 JINST 7 C02019

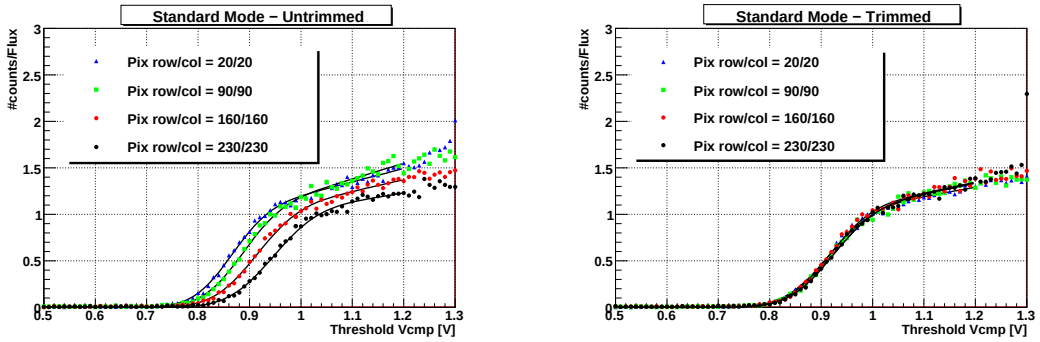

(a) (b)

Figure 4. S-curves for 4 pixels with trim bits=32 (a) and after trimming (b).

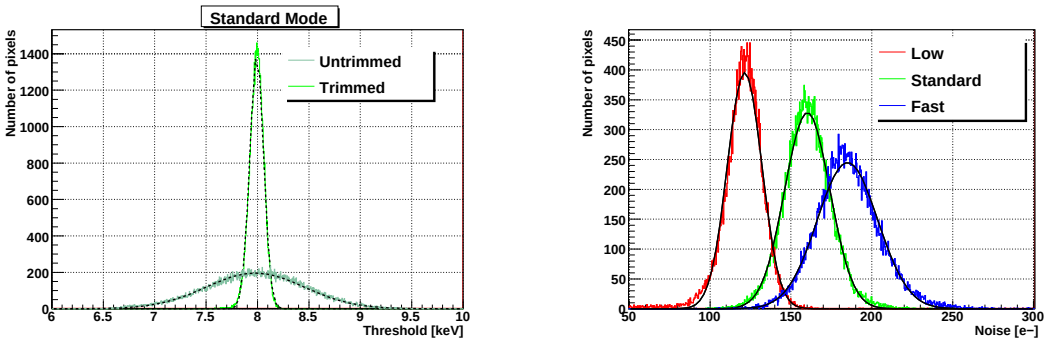

(a) (b)

Figure 5. (a) Threshold dispersion before and after trimming measured in *Standard mode* of operation of the chip and with X-ray from fluorescence on Cu. (b) Noise distribution in the three modes of operation.

In figure 5 the noise in the three different gain modes is compared, the noise values are shown in table 1. As expected, the *Low noise mode* with the highest gain of the preamplifier generates less noise, while fast, smaller signals generated by the preamplifier in a low gain configuration are noisier.

3.5 Rate capability

The performance of EIGER at high photon fluxes has also been investigated. A typical feature of a counting detector, that affects the counting capabilities at high photon fluxes, is the pile up of signals from photons arriving on the same pixel too close in time. When a second charge impulse arrives before the previous one has gone below the comparator threshold, only one pulse is counted. The return to zero time of the signal is strictly related to the relative threshold level and to the preamplifier gain: the higher the gain the longer the return to zero time.

The rate capability of EIGER has been measured at three different gain settings with monochromatic beam at Optics beam line. For this measurement the time structure of the photon delivery, related to the electron distribution in the beam, has to be taken into account. Nevertheless, a flat-filled synchrotron beam is considered to be a good approximation of the actual beam structure at PSI-SLS [9]. In this simplified model, the loss in counting efficiency at high rate can

2012 JINST 7 C02019

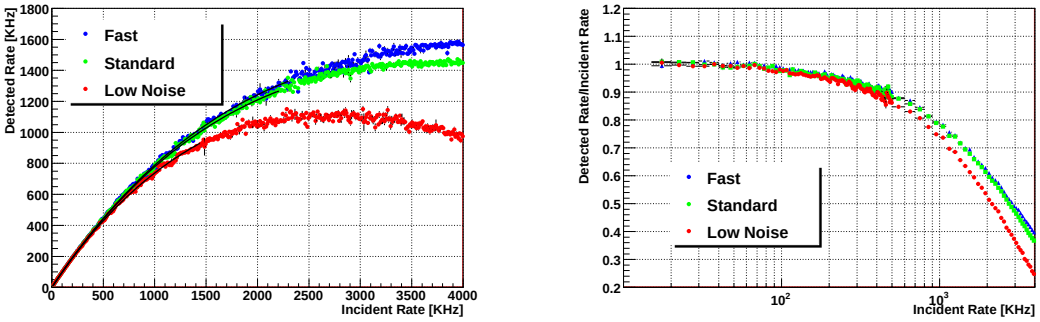

(a) (b)

Figure 6. (a) Detected count rate of a pixel in kHz as a function of incident rate for monochromatic beam of 16 keV (b) Pixel efficiency (detected/measured rate) as a function of incident rate for monochromatic beam of 16 keV. Measurements performed at the Optics beam line.

be calculated with eq. (3.2) [10]:

$$N_{\rm obs} = N_0\, e^{(-N_0\tau)} \tag{3.2}$$

where $N_{\rm obs}$ and N_0 are the measured and the incident photon rate respectively, and τ is the dead time of the chip. The rate of measured counts versus the rate of incident photons is fitted with eq. (3.2) to extract the chip dead time. Once τ is measured at different settings, the same equation can be used to correct the measured rate. At photon flux of $N_0^{\rm max} = 1/\tau$ the curve described by eq. (3.2) reaches a maximum and beyond this point there is no longer a distinct correspondence between N_0 and $N_{\rm obs}$.

To control the beam intensity, two filter wheels equipped with Al sheets of different thickness have been combined. To avoid beam hardening due to absorbers, a beam energy of 16 keV, with low contamination of the higher harmonic, has been chosen. In addition, the thinnest Al thickness (2.2 mm with an attenuation factor of 97.4%) able to reduce the flux in a region where the chip has a linear response was used as reference. In each mode of operation the global threshold $V_{\rm cmp}$ has been set to the half photon energy: 8 keV. The direct unfocused synchrotron beam has been scattered on a carbon foil to distribute the flux accross the whole chip with a gradient from $4x10^4$ counts/pixel/s in the highest flux region down to 10 counts/pixel/s in the beam periphery.

Figure 6-(a) shows the measured rate on each pixel in direct beam as a function of the measured rate with 2.2 mm Al sheet. In figure 6-(b) the pixel efficiency, defined as the detected rate divided by the measured, is plotted as a function of the incident rate. Both plots show that in all the settings the efficiency is greater than 95% up to $\simeq$ 200 kHz. In the worst case (*Low noise mode*) a rate correction could be applied until 2 MHz. The dead times, extracted from the fit with eq. (3.2), are reported in the last column of table 1.

3.6 Radiation tolerance

The irradiation was performed at the synchrotron beam line with a defocused photon monochromatic beam of 14 keV. A pixel region of $\simeq$ 7 mm^2 ($\simeq$1300 pixels) was irradiated in steps up to a dose of $\simeq$ 6 MRad, while a chip portion containing part of the row shift register and of the column periphery was irradiated up to $\simeq$ 16 MRad. Functionality tests of the chip after irradiation show that the chip can be operated at full readout speed with minor adaption of the chip readout

2012 JINST 7 C02019

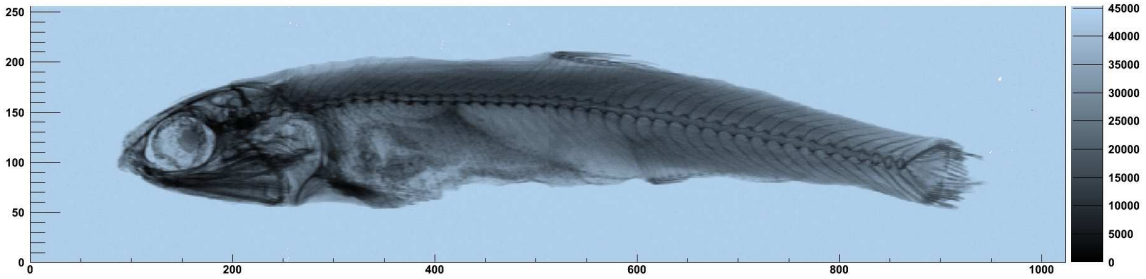

Figure 7. First X-ray image of an 1/2 EIGER module (number of pixels 260000).

parameters. The irradiated pixels show a difference in the comparator threshold with respect to the pre-irradiated level, which increases as a function of the dose. Even at the highest dose, the thresholds of the irradiated pixels can be still equalised to the not irradiated one by increasing the trim bit voltage to $V_{\text{trim}} = 1.2$ V. Further measurements of the noise and rate capability of the irradiated pixels are planned.

4 Summary and conclusions

EIGER is a new single photon counting pixel detector for synchrotron radiation developed at PSI. It is characterized by a small pixel size 75×75 μm^2 and high frame rate capability up to 23 kHz. The three modes of operation of the chip: *Low noise*, *Standard* and *Fast* have been characterized. Overall the general behavior of the chip is in agreement with expectation and the chip has shown good performance: with 6 trim bit DACs it is possible to lower the threshold dispersion to 70 eV. For high rate experiments the *Fast mode* achieves a minimum dead time of 238 ns; while for low energy photon detection the *Low noise mode* is showing a noise of $\simeq 430$ eV or $\simeq 120$ e$^-$ and a minimum energy threshold of 4 keV. A further higher gain setting could be used in order to detect even lower energy photons of 2.5 keV, a detailed characterization of this *Very low noise mode* of operation of the chip has to be performed. In particular the noise and the rate capability have to be measured.

Concerning the module production all the components for the module control and readout (FEB, BEB, HDI) are produced and tested. Due to the high number of pixels on a chip and the small pixel size, the bump-bonding of eight chips to a Si sensor is a challenge. A refurbishing of the bump-bonding machine to match EIGER features was done.

A first step towards the module is the read out of a half module; four chips, covering a sensitive area of $\simeq 2 \times 8$ cm^2, have been connected to the readout chain. Figure 7 shows the first X-ray (Cu tube) image of a dried anchovy. For this measurements no trimming was performed but a *Flat Field* correction[1] has been applied to take into account the pixel to pixel variations and the beam profile. The image quality and the level of details are very impressive and show the high resolution capabilities of EIGER. Moreover, only few pixels are insensitive to photons (white spots in the image) proving good yield of the bump-bonding process.

[1]Two successive images are taken, with and without the object, the final one is obtained dividing pixel by pixel the counts measured with the object by the counts without.

2012 JINST 7 C02019

Acknowledgments

The authors would like to thank the staff of the PSI SLS-Optics beamline (X05DA): Uwe Flechsig and Peter Oberta for their support during the measurements. Many thanks also to Dhanya Maliakal, Lukas Schaedler and Christian Ruder of PSI SLS Detector group for their support both in the experimental setup and in the EIGER production. Thanks to ESRF for the financial support.

References

[1] R. Dinapoli et al., *EIGER: next generation single photon counting detector for X-ray applications*, *Nucl. Instrum. Meth.* **A 650** (2011) 79.

[2] B. Henrich et al., *PILATUS: a single photon counting pixel detector for X-ray applications*, *Nucl. Instrum. Meth.* **A 607** (2009) 247.

[3] A. Bergamaschi et al., *The MYTHEN detector for X-ray powder diffraction experiments at the Swiss Light Source*, *J. Synchrotron Radiat.* **17** (2010) 653.

[4] O. Bunk et al., *Multimodal X-ray scatter imaging*, *New J. Phys.* **11** (2009) 123016.

[5] I. Johnoson et al., *A Geiger-mode avalanche photodiode array for X-ray photon correlation spectroscopy*, *J. Synchrotron Radiat.* **16** (2009) 105.

[6] I. Johnson et al., *Coherent diffractive imaging using phase front modifications*, *Phys. Rev. Lett.* **100** (2008) 155503.

[7] U. Flechsig, A. Jaggi, S. Spielmann, H.A. Padmore and A.A. MacDowell, *The optics beamline at the Swiss Light Source*, *Nucl. Instrum. Meth.* **A 609** (2009) 281.

[8] P. Kraft et al., *Characterization and calibration of PILATUS detector*, *IEEE Trans. Nucl. Sci.* **56** (2009) 758.

[9] B. Sobott et al., *Matching detector performance to source profile to optimise detector linearity*, to be published on *JINST*, in *Proceedings of* "13$^{\text{th}}$ *International Workshop on Radiation Imaging Detectors"*, ETH, Zurich Switzerland July 3–7 2011.

[10] P. Kraft et al., *Performance of single photon counting PILATUS detector modules*, *J. Synchrotron Radiat.* **16** (2009) 368.

2012 JINST 7 C02019